

# Assessing the work budget and efficiency of fault systems using mechanical models

Michele L. Cooke and Susan Murphy

Geosciences Department, University of Massachusetts, Amherst, Massachusetts, USA

Received 7 January 2004; revised 13 July 2004; accepted 26 July 2004; published XX Month 2004.

[1] We examine the work energy budget of actively deforming fault systems in order to develop a means of examining the systemic behavior of complex fault networks. Work done in the deformation of a faulted area consists of five components: (1) work done against gravity in uplift of topography ( $W_{\text{grav}}$ ); (2) internal energy of the strained host rock ( $W_{\text{int}}$ ); (3) work done resisting friction during slip on faults ( $W_{\text{fric}}$ ); (4) seismic energy released in earthquake events as ground shaking ( $W_{\text{seis}}$ ); and (5) work done in initializing new faults and propagating existing faults ( $W_{\text{prop}}$ ). The energy budget of a fault system can be expressed as  $W_{\text{TOT}} = W_{\text{grav}} + W_{\text{int}} + W_{\text{fric}} + W_{\text{seis}} + W_{\text{prop}}$ . For a balanced energy budget the total of these five components will equal the external tectonic work applied to the system. We examine the work balance within hypothetical and simulated two-dimensional static fault systems using mechanical models. The boundary element method models produce a balanced work budget for both simple and complex fault system models. The presence of slipping faults reduces the internal strain energy of the faulted area ( $W_{\text{int}}$ ), at a “cost” of work done against friction and gravity (and propagation and seismic energy, where applicable). Calculations of minimum work deformation match expected deformation paths, indicating the usefulness of this approach for evaluating efficiency in more complex systems. The partitioning of various work terms may express the relative efficiency or maturity of fault systems. Furthermore, calculation of potential seismic energy release can provide an upper bound to earthquake seismic moment assessments. **INDEX TERMS:** 8010 Structural Geology: Fractures and faults; 8020 Structural Geology: Mechanics; 8123 Tectonophysics: Dynamics, seismotectonics; 8122 Tectonophysics: Dynamics, gravity and tectonics; **KEYWORDS:** work minimization, fault system growth, mechanical models

**Citation:** Cooke, M. L., and S. Murphy (2004), Assessing the work budget and efficiency of fault systems using mechanical models, *J. Geophys. Res.*, 109, XXXXXX, doi:10.1029/2004JB002968.

## 1. Introduction

[2] Geologic faults rarely occur in isolation but develop within interacting systems of faults. Consequently, understanding the behavior (i.e., slip distribution, slip rates and growth) of any one fault requires consideration of the entire system. Field and numerical studies have shown that interacting faults have slip distributions different from those along equivalent isolated faults [Willense and Pollard, 2000; Maerten et al., 1999; Savage and Cooke, 2004]. Such differences may have important implications for the prediction of seismic hazards and understanding fault system evolution. Earthquake triggering studies, for example, have demonstrated that an earthquake on one fault can change the probability of earthquakes on nearby faults [e.g., King et al., 1994; Harris, 1998; Stein, 1999]. Other studies have shown that fault systems evolve through the growth, interaction and linkage of individual fault segments [e.g., Gupta et al., 1998; Dawers and Underhill, 2000; Kattenhorn and Pollard, 2001; Mansfield and Cartwright, 2001; Childs et al., 2003].

[3] We explore a method for analysis of an entire system of faults based on the work budget of the fault system. The distribution of work energy among forms of deformation, such as internal strain in the surrounding rock, topographic uplift, frictional slip and creation of new fault surfaces, can aid our understanding of the mechanical behavior and evolution of a fault system as a whole. For example, new fault surfaces develop at a work energy “cost” that must be compensated for, either in terms of reduced internal strain or an increase in the total tectonic work input into the system. The total work for each form of deformation provides a quantitative means to assess the behavior of the entire fault system. In this way, locally destructive or constructive fault interactions may be tempered by their role within the larger system. Investigation of work within a system of active faults assesses behavior that pertains to timescales that bridge those of single earthquakes and geologic deformation, thus providing critical insight into behavior of active fault systems.

### 1.1. Work Budget and Efficiency

[4] Work analyses of geologic processes have often been applied to assess the relative efficiency of alternative paths

of deformation [Masek and Duncan, 1998; Jamison, 1993; Dahlen and Barr, 1989; Molnar and Lyon-Caens, 1988; Mitra and Boyer, 1986; Sleep et al., 1979]. These efficiency-based or minimum work analyses rely on the proposition that deformation will occur to minimize the work required to accommodate the tectonic strain. The work budgets of deforming fold-and-thrust belts have been analyzed by analogy to wedges of soil or snow that deform in front of a moving bulldozer; these analyses utilize the premise that the deforming wedge grows by minimizing the work done [Dahlen and Barr, 1989]. Mitra and Boyer [1986] used a minimum work criterion to assess the tendency of foreland duplexes to deform via slip on existing faults or by creation of new faults. Jamison [1993] relied on minimum work to explain the conditions under which triangle zones will form. Masek and Duncan [1998] explored the effect of friction and topography on the evolution of orogenic zones using minimum work techniques. Minimum work analyses have also been applied to predict the orientation of spreading ocean ridges and transforms [Sleep et al., 1979] and explain the lateral expansion of continental platforms [Molnar and Lyon-Caens, 1988]. Our mechanical analysis, based on the approach of Mitra and Boyer [1986], extends from previous work by (1) including work components directly related to fault slip, such as strain concentration around fault tips and energy released in earthquakes, and (2) permitting evaluation of complexly interacting fault systems that are difficult to evaluate using the analytical methods cited above.

[5] Elements of a fault system's work budget, such as internal strain energy, have been used in conjunction with geologic data to evaluate between alternative fault systems [Cooke and Kameda, 2002; Griffith and Cooke, 2004]. However, these studies considered neither the inelastic components of several work terms nor the gravitational work of fault systems. Our rigorous balance of work budget components presented here provides a more complete tool for the analysis of alternative fault systems as well as fault system evolution.

[6] This paper presents each of the terms in the work budget, followed by two-dimensional analysis of an isolated single fault and a simple two-fault system under horizontal contraction. After building our intuition with the single-fault and two-fault models, we apply the work budget to the complexly interacting faults of the Los Angeles basin with a two-dimensional analysis. The insights gained by these two-dimensional analyses can also be applied to three-dimensional systems, although such applications are beyond the scope of this paper.

## 2. Work Budget of a Fault System

[7] Work done in the deformation of a faulted area consists of five components, shown in Figure 1 for the case of an idealized single fault system undergoing contraction. First, work is done against gravity in uplift of topography ( $W_{\text{grav}}$ ). This term can be negative where deformation decreases elevation. Second, work is done in straining the host rock surrounding the fault. We refer to this work as the internal strain energy ( $W_{\text{int}}$ ). Third, when a fault slips, work is done resisting friction along the fault surface ( $W_{\text{fric}}$ ). Heat energy resulting from frictional slip is taken into account within the  $W_{\text{fric}}$  term.  $W_{\text{fric}}$  will be zero for a frictionless

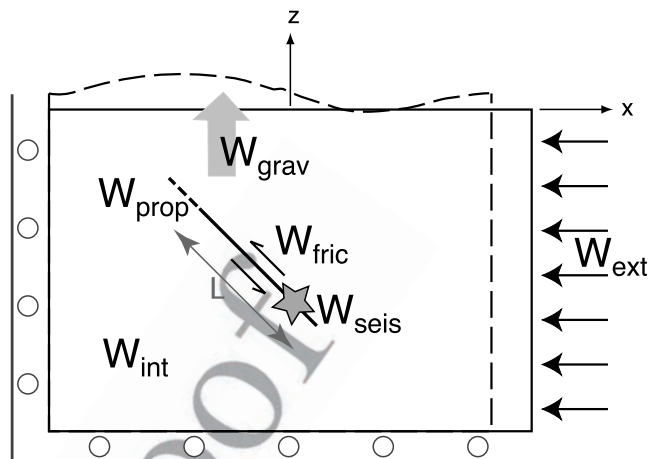


**Figure 1.** Conceptualization of work components within an idealized single-fault system under horizontal contraction. The left and bottom boundaries are allowed to slide but do not permit normal displacement. The dashed lines represent the shape of the conceptual model boundaries and fault after deformation and propagation. The work of internal strain ( $W_{\text{int}}$ ) work against gravity ( $W_{\text{grav}}$  and large gray arrow) work against friction along the fault ( $W_{\text{fric}}$  and small arrows) work of fault propagation ( $W_{\text{prop}}$ ), work of seismic energy released ( $W_{\text{seis}}$  and star) and external work ( $W_{\text{ext}}$  and horizontal arrows) are shown schematically.

fault. Fourth, where fault slip takes the form of earthquake events, seismic energy is lost from the system in the form of ground motion ( $W_{\text{seis}}$ ). Finally, work is done in initializing new faults and propagating existing faults ( $W_{\text{prop}}$ ). This work depends on the amount of new fracture surface area produced. The energy budget of the system can thus be expressed as:

$$W_{\text{TOT}} = W_{\text{fric}} + W_{\text{int}} + W_{\text{grav}} + W_{\text{seis}} + W_{\text{prop}}, \quad (1)$$

where  $W_{\text{TOT}}$  is the total energy consumed during deformation.

[8] We consider each of these components in turn, using a simple two-dimensional single fault for illustration (Figure 1). Each of these work terms is first formulated in three dimensions and then simplified to two dimensions for application to the numerical models of this study. The two dimensional analysis demonstrates the effectiveness of this methodology for analyzing fault systems and can be extended to three dimensions when the appropriate Boundary Element Method (BEM) tools are available.

### 2.1. Work Against Gravity

[9] Regional contractional strain results in a net increase in elevation of the region. Although localities within a contracting mountain belt may experience local extension and associated downdrop, the overall vertical movement of the deforming region is upward. This requires that work be done against gravity. Conversely, in extensional regimes, the overall work against gravity is negative, indicating that

work is being done by gravity; that is, gravity contributes to the extensional deformation.

[10] Even in the absence of faulting, horizontal contraction produces increased elevation through vertical dilation of rock material, expressed by the material's Poisson's ratio. In addition, slip on faults under horizontal contraction results in movement of the hanging wall up the fault ramp against the force of gravity. There may also be downward movement of the footwall, but the hanging wall generally has greater upward displacement than the footwall downward because the shallower material has less overburden to resist deformation. Although not considered explicitly in this study, in extension overall elevation decreases as the hanging wall moves down the footwall. A complete calculation of work done by gravity must account for all of these effects.

[11] We calculate all work against gravity by considering the change in gravitational potential energy between the initial, undeformed state and the final deformed state. Because gravitational work is conservative and not path-dependent, we need consider only the final deformation state. This is not the case for all of the work components. The change in gravitational potential energy at a point,  $\Delta U_g$ , is

$$W_g = \Delta U_g = m g d_z \quad (2)$$

where  $m$  is the mass being displaced,  $g$  is the gravitational constant, and  $d_z$  is the vertical displacement of the point [e.g., *Young and Freedman*, 1996].

[12] In a deforming region, the vertical displacement will vary with both horizontal position and with depth,  $z$ . The mass displaced by the vertical displacement varies with depth based on the density,  $\rho$ , so that a column with length  $dx$  and width  $dy$  will have a mass  $\rho z dx dy$ . The total gravitational work is then

$$W_{\text{grav}} = \iiint \rho g d_z(z) dz dx dy, \quad (3)$$

where  $x$  and  $y$  give the horizontal position and  $z$  the depth of the point in the undeformed state. We use  $\rho$ ,  $x$ ,  $y$ , and  $z$  from the undeformed state because the mass of the column of rock,  $\rho z dx dy$ , remains constant although both the shape of the column and density change in response to contraction; that is

$$\rho z dx dy = \rho' z' dx' dy', \quad (4)$$

where the superscript indicates the deformed state. In the two-dimensional case we consider a cross-section of unit width, so that equation (3) becomes

$$W_{\text{grav}} = \iint \rho g d_z(z) dz dx. \quad (5)$$

## 2.2. Work Done in Internal Strain of the Host Rock

[13] Tectonic stresses also perform work in the form of internal strain within the rock surrounding the fault, referred to as the internal strain energy of the rock [*Timoshenko and*

*Goodier*, 1934]. *Timoshenko and Goodier* [1934] derive a general formula for internal strain energy, based on summing the work done by the local stress and strain for an infinitely small increment of strain. For example, in the horizontal  $x$  direction

$$dW_{xx} = \sigma_{xx} dy dz \epsilon_{xx} dx, \quad (6)$$

where  $\sigma_{xx}$  is the horizontal stress in the  $x$  direction,  $dy dz$  is the area over which the stress acts,  $\epsilon_{xx}$  is the strain in the  $x$  direction, and  $dx$  is the length subject to the strain. In contrast to the gravitational term, the stresses vary with strain, so that the incremental work calculated above must be integrated over the entire strain. This integral can be simplified if we assume that the rock behaves linearly-elastically, which is realistic for infinitesimal strains (under 1%) such as characteristic of earthquake recurrence time-scales. Then,

$$\int \sigma_{ij} \epsilon_{ij} = \frac{1}{2} \sigma_{ij} \epsilon_{ij}. \quad (7)$$

This is in contrast to frictional work and external work; for those terms stress depends on strain but is not linear so that the integral cannot be simplified. Summing over all six components of stress gives a total work of

$$dW = V_0 dx dy dz, \quad (8a)$$

where

$$V_0 = 1/2(\sigma_{xx}\epsilon_{xx} + \sigma_{yy}\epsilon_{yy} + \sigma_{zz}\epsilon_{zz} + 2\sigma_{xy}\epsilon_{xy} + 2\sigma_{yz}\epsilon_{yz} + 2\sigma_{xz}\epsilon_{xz}). \quad (8b)$$

$V_0$  is the amount of work per unit volume, or strain energy density [*Timoshenko and Goodier*, 1934].

[14] Strain energy density (SED) measures the elastic strain energy stored at any point within the host rock. We expect that SED will vary systematically in response to slip on faults. SED shadows may develop adjacent to slipping faults where the strain within the rock has lessened and SED may concentrate in locally deformed areas, such as around fault tips. SED analysis has been applied to evaluate shear fracture propagation in en echelon fault arrays [*Du and Aydin*, 1993] and to evaluate the mechanical efficiency of alternative fault interpretations [*Cooke and Kameda*, 2002; *Griffith and Cooke*, 2004].

[15] The plane strain conditions for our two-dimensional fault system ( $\epsilon_{yy} = \epsilon_{xy} = \epsilon_{yz} = 0$ ) reduce the expression to only three terms. To further simplify the strain energy expression, we can apply the elastic constitutive equations to express  $V_0$  in terms of only stress and elastic properties  $E$  (Young's modulus) and  $\nu$  (Poisson's ratio).

$$V_0 = \frac{(1-\nu^2)}{2E}(\sigma_{xx}^2 + \sigma_{zz}^2) + \frac{(1+\nu)}{E}(\sigma_{xz}^2 + \nu\sigma_{xx}\sigma_{zz}). \quad (9)$$

[16] In examining the work budget of an entire fault system, we are concerned with the total work consumed in the form of internal strain energy,  $W_{\text{int}}$ . Because SED



261 varies across a faulted area, the total work  $W_{\text{int}}$  is calculated  
262 by summing over the entire area

$$W_{\text{int}} = \iint V_0(x, z) dx dz. \quad (10)$$

### 265 2.3. Work Against Friction

266 [17] When a fault slips in response to a tectonic strain,  
267 work is done resisting friction along the fault surface. The  
268 frictional resistance stress,  $\tau_{\text{fric}}$ , is a component of the shear  
269 stress along the fault and equals the fault's friction coeffi-  
270 cient,  $\mu$ , multiplied by stress normal to the fault,  $\sigma_N$ , for any  
271 compressive normal stress ( $\sigma_N < 0$ ); for a zero or tensile  
272 normal stress,  $\tau_{\text{fric}}$  always equals 0. The total shear stress  
273 along the fault includes any shear stress induced by gravity,  
274 which is accounted for in  $W_{\text{grav}}$ . For any one segment of the  
275 fault with area  $dA$  the frictional work,  $W_{\text{fric}}$ , is generalized as

$$W_{\text{fric}} = -\sigma_N \mu s dA, \quad \sigma_N < 0, \quad (11a)$$

$$W_{\text{fric}} = 0, \quad \sigma_N \geq 0, \quad (10b)$$

279 where  $\sigma_N$  is the normal stress across the fault,  $dA$  is the area  
280 of the fault segment,  $\mu$  is the friction coefficient, and  $s$  is  
281 slip. For freely slipping faults,  $\mu = 0$  and no work is done  
282 against friction. Both  $\sigma_N$  and  $s$  may vary along the length of  
283 the fault. Work done along the whole two-dimensional fault  
284 of length  $l$  (Figure 1) during an increment of slip can be  
285 expressed as

$$W_{\text{fric}} = \int_0^L \sigma_N(l) \mu s(l) dl. \quad (12)$$

287 In addition, the normal stress and slip will vary as the  
288 tectonic strain varies, and as increased topography over the  
289 fault increases lithostatic compression. Consequently,  $\sigma_N$   
290 and  $s$  depend on the horizontal tectonic strain  $\epsilon_{\text{hor}}$  and the  
291 complete work term in two dimensions,

$$W_{\text{fric}} = \iint \sigma_N(\epsilon_{\text{hor}}, l) \mu s(\epsilon_{\text{hor}}, l) d\epsilon_{\text{hor}} dl, \quad (13)$$

293 incorporates both an integration along the fault length as  
294 well as an integration along tectonic loading path. In  
295 contrast to the nonstrain path-dependent treatment of the  
296 internal strain energy term,  $W_{\text{int}}$ , we must consider the strain  
297 integral in calculation of  $W_{\text{fric}}$  because the dependency of  $\sigma_N$   
298 and  $s$  on the tectonic strain is not linear. Although the  
299 material may be assumed linear elastic, the presence  
300 of frictional faults supplies nonlinearity to the system. The  
301 frictional work is also nonconservative; work done resisting  
302 friction is converted to heat and absorbed by the surround-  
303 ing rock. Heat flux measured near the earth's surface can be  
304 used to assess the frictional resistance of active faults  
305 [Scholz, 2002].

### 306 2.4. Seismic Energy

307 [18] In addition to the work that is expressed as observ-  
308 able deformation, energy may be consumed in an actively

deforming region through seismic energy lost to the envi- 309  
ronment in the form of ground motion during earthquake 310  
events,  $W_{\text{seis}}$ . This term is related to the seismic moment. 311  
The seismic energy released for a two-dimensional fault of 312  
length  $l$  is 313

$$W_{\text{seis}} = \iint \Delta\tau(\epsilon_{\text{hor}}, l) s(\epsilon_{\text{hor}}, l) d\epsilon_{\text{hor}} dl, \quad (14)$$

where  $\Delta\tau$  is the change in shear stress associated with fault 315  
slip and  $s$  is slip [e.g., Scholz, 2002]. Once again slip, as 316  
well as shear stress drop, depends on the tectonic strain,  $\epsilon_{\text{hor}}$ , 317  
so that seismic work must be integrated over the loading 318  
path. 319

[19] If faults are permitted to slip wherever the shear 320  
stress exceeds a constant frictional resistance ( $\sigma_N \mu$ ), slip 321  
occurs without earthquake events, and the fault creeps. In 322  
that case, the shear stress is maintained at the level of 323  
frictional resistance, so that there is no shear stress drop, and 324  
 $W_{\text{seis}}$  equals zero. Seismic energy of earthquakes is associ- 325  
ated with stick slip, where the friction coefficient on the 326  
fault surface is reduced as the fault slips. Rate and state 327  
friction theory demonstrates the release of seismic energy 328  
with drop of friction coefficient from static to dynamic 329  
levels [e.g., Marone, 1998]. The opposing end-member to a 330  
creeping fault is a fault that releases all of its accumulated 331  
shear stress within one earthquake event. The seismic 332  
energy calculated along such a fault represents the maxi- 333  
mum possible energy released over the time considered. 334

### 2.5. Work Initializing and Propagating Faults 335

[20] The work done in initializing new faults and prop- 336  
agating existing faults,  $W_{\text{prop}}$ , can be calculated using the 337  
surface energy of a crack,  $\gamma$ , the energy per unit area 338  
required to break the bonds of the material [e.g., Scholz, 339  
2002; Lawn and Wilshaw, 1975]. Experimental studies have 340  
shown that the critical surface energy values for fault 341  
propagation depend on normal compression and range from 342  
 $10^1$  to  $10^4$  J m<sup>-2</sup> [Wong, 1982, 1986; Cox and Scholz, 343  
1988]. These experiments consider the surface area created 344  
by microcracking adjacent to sliding fault surfaces.  $W_{\text{prop}}$  345  
for the fault system depends on the total surface area created 346  
during fault growth; this includes not only the primary fault 347  
surface and associated microcracks but also the surface 348  
areas within a zone of cataclasite along the fault [Scholz, 349  
2002; Mitra and Boyer, 1986]. This cataclastic zone 350  
includes macroscale faults. The complete relationship can 351  
be expressed as 352

$$W_{\text{prop}} = \gamma p + \gamma p w r, \quad (15)$$

where  $\gamma$  is the surface energy per unit length,  $p$  is the added 354  
length of the fault,  $w$  is the width of the cataclasite zone, and 355  
 $r$  is the density of secondary faults in the zone [Mitra and 356  
Boyer, 1986]. 357

### 2.6. Total Work and External Work on the System 358

[21] The total work done within the system is the sum of 359  
all five of the components discussed above. A summary of 360  
the formula of the work components in two dimensions is 361  
set forth in Table 1. 362

t1.1 **Table 1.** Formula for Each Work Component in Two Dimensions

t1.2	Work Component	Symbol	Characteristics	Two-Dimensional Formulation
t1.3	Work against gravity	$W_{\text{grav}}$	conservative, nonpath-dependent	$\iint \rho g d_z(z) dz dx$
t1.4	Internal strain energy	$W_{\text{int}}$	conservative, linear-elastic, nonpath-dependent	$\iint V_0(x, z) dz dx$
t1.5	Work against friction	$W_{\text{fric}}$	nonconservative, nonlinear, path-dependent	$\iint \sigma_N(\epsilon_{\text{hor}}, l) \mu s(\epsilon_{\text{hor}}, l) d\epsilon_{\text{hor}} dl$
t1.6	Seismic energy	$W_{\text{seis}}$	nonconservative, nonlinear, path-dependent	$\iint \Delta \tau(\epsilon_{\text{hor}}, l) s(\epsilon_{\text{hor}}, l) d\epsilon_{\text{hor}} dl$
t1.7	Work creating new fault surface	$W_{\text{prop}}$	nonconservative, nonpath-dependent	$\gamma p + \gamma p w r$
t1.8	External work	$W_{\text{ext}}$	nonconservative, nonlinear, and path-dependent	$\int \sigma_{\text{hor}}(\epsilon_{\text{hor}}, z) A \epsilon_{\text{xx}}(z) d\epsilon_{\text{hor}} dz$

363 [22] Finally, if the far field tectonic stress or strain can be  
 364 well defined along an appropriate boundary of the system,  
 365 the total work done in the system,  $W_{\text{TOT}}$ , equals the work  
 366 done on the external boundary of the system,  $W_{\text{ext}}$ , under the  
 367 principle that work done on the boundary of a closed system  
 368 equals the increase in energy within the system [e.g., *Young*  
 369 *and Freedman*, 1996]. Within geological systems, such  
 370 boundaries may be plate margin boundaries or zones where  
 371 strain rates are known from geodesy. Again using our  
 372 simple application of a constant horizontal tectonic strain,  
 373  $\epsilon_{\text{hor}}$ , the stress,  $\sigma_{\text{hor}}$ , along the boundary depends on this  
 374 tectonic strain as well as depth,  $z$ . The complete work term  
 375 in two dimensions is

$$W_{\text{ext}} = \iint \sigma_{\text{hor}}(\epsilon_{\text{hor}}, z) A \epsilon_{\text{xx}}(z) d\epsilon_{\text{hor}} dz, \quad (16)$$

377 where  $A$  is the area of the external boundary (boundary  
 378 height in two dimensions). As with  $W_{\text{fric}}$ , the nonlinearity of  
 379 the slipping fault system necessitates consideration of the  
 380 strain path integral, since the dependence of stress on degree  
 381 of strain is not linear. Requiring that external work equal the  
 382 sum of the work components outlined above provides an  
 383 important check on a complete work balance equation, and  
 384 provides a single measure with which to assess the total  
 385 work expended in the deformation of a region.

### 387 3. Evaluating Fault System Work Components 388 Using Mechanical Modeling Tools

389 [23] The work components outlined above can be calcu-  
 390 lated for a variety of fault systems using analytical or  
 391 numerical mechanical models. Numerical methods such as  
 392 finite element method (FEM) and boundary element method  
 393 (BEM) can simulate deformation associated with complex  
 394 fault configurations by calculating stress and strain through-  
 395 out a body due to prescribed tractions or displacements on  
 396 the model boundaries, using the principles of continuum  
 397 mechanics [e.g., *Crouch and Starfield*, 1990]. All the data  
 398 necessary for the analysis, including slip, traction, internal  
 399 stress and strain and vertical displacements, are constrained  
 400 by the governing differential equations of continuum me-  
 401 chanics. A comparison of numerical results to analytical  
 402 solutions for simple situations provides a means of assess-  
 403 ing the error of numerical results.

404 [24] This study utilizes BEM models. Unlike FEM, which  
 405 requires discretization of the entire body, BEM only  
 406 requires discretization of model boundaries and discontinu-  
 407 ities (i.e., faults). This is advantageous for modeling mul-  
 408 tiple interacting faults because BEM requires less effort for  
 409 discretization, and errors due to discretization and approx-  
 410 imation arise only on the boundaries and along fault  
 411 surfaces [*Crouch and Starfield*, 1990].

[25] This study employs a two-dimensional BEM code, 412  
 FRIC2D, that computes elastic and inelastic deformation 413  
 associated with frictional slip along faults using the dis- 414  
 placement discontinuity formulation of *Crouch and* 415  
*Starfield* [1990] with special constitutive frictional slip 416  
 elements [*Cooke and Pollard*, 1997]. The model boundaries 417  
 and fault are discretized into linear elements each with 418  
 uniform shear and normal displacement discontinuities. 419  
 The models are finite and the position and orientation of 420  
 the model boundaries can be prescribed to simulate a wide 421  
 range of conditions. For example, nonrectangular bound- 422  
 aries have been used to simulate deformation over buried 423  
 craters on Mars [*Buczkowski and Cooke*, 2004]. Addition- 424  
 ally, fault geometry is prescribed by the positions and 425  
 orientations of the fault elements. FRIC2D requires pre- 426  
 scription of the faults' constitutive properties (i.e., frictional 427  
 strength) [*Cooke and Pollard*, 1997]. FRIC2D has been 428  
 used to investigate the early stages of fault-related fold 429  
 development [*Cooke and Pollard*, 1997], bedding plane slip 430  
 within folds [*Cooke et al.*, 2000], joint propagation near 431  
 bedding planes [*Cooke and Underwood*, 2001], and blind 432  
 thrust fault propagation [*Roering et al.*, 1997]. 433

[26] FRIC2D incorporates idealizations that do not reflect 434  
 all geological conditions. The models assume a linear elastic 435  
 rheology that omits time-dependent viscoelastic effects that 436  
 may be important on long timescales [e.g., *Rundle*, 1982; 437  
*Cohen*, 1984]. The models also assume homogeneous and 438  
 isotropic material properties, a potentially major simplifica- 439  
 tion depending on the rock types in the area of concern. 440  
 This technique therefore captures only the first-order effects 441  
 of fault configuration on work; differences due to rock 442  
 rheology must be assessed independently. 443

#### 3.1. Model Setup 444

[27] To illustrate this analysis, we again consider the case 445  
 of a single fault under contraction, as modeled using the 446  
 BEM code FRIC2D (Figures 1 and 2). The rock surround- 447  
 ing the fault is homogeneous, linear elastic and isotropic. 448  
 The material properties used were chosen based on the rock 449  
 types in the Los Angeles basin for consistency with models 450  
 presented in section 8; these values represent an average 451  
 over a range of sedimentary, metamorphic and igneous rock 452  
 types [*Cooke and Kameda*, 2002] A uniform leftward 453  
 displacement is applied to the right hand boundary of the 454  
 model to produce 1% contractional strain across the model. 455  
 A bilateral gravitational stress field is superposed on the 456  
 model with 457

$$\sigma_{zz} = \rho g z \quad (17a)$$

$$\sigma_{xx} = \frac{\nu}{1 - \nu} \rho g z, \quad (17b)$$

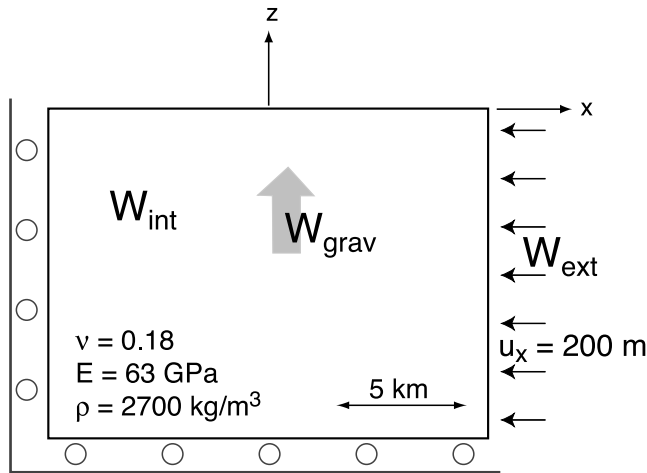


**Figure 2.** Configuration of the faultless model used to compare the boundary element method results with the analytical solution. Material properties, Poisson's ratio,  $\nu$ , Young's modulus,  $E$ , and density,  $\rho$ , are shown. The model is contracted by displacement of the right boundary 200 m to the left. The only nonzero work terms are external work,  $W_{\text{ext}}$ , internal work,  $W_{\text{int}}$ , and work against gravity,  $W_{\text{grav}}$ .

where  $\rho$  is density,  $g$  is gravitational acceleration,  $\nu$  is Poisson's ratio,  $x$  is horizontal position and  $z$  is elevation (negative below the surface); compressional stress is negative. The nonuniform  $\sigma_{xx}$  prevents heterogeneous lateral expansion of the model that results from lithostatic ( $\sigma_{xx} = \sigma_{zz} = \rho gz$ ) stress state [e.g., Engelder, 1993; Jaeger and Cooke, 1976]. For the first few sets of models (sections 4 and 5), the system is static; the fault is not permitted to propagate and no additional faults may initiate (i.e.,  $W_{\text{prop}} = 0$ ). In addition, the fault slips whenever the shear stress on the fault exceeds the frictional resistance, and does not experience earthquake events (i.e.,  $W_{\text{seis}} = 0$ ). This analysis does however provide implications for  $W_{\text{seis}}$ , discussed later in this paper (sections 6, 8, and 9).

[28] The inelastic nature of the fault system results in the loading path dependencies of several work terms (e.g.,  $W_{\text{fric}}$  and  $W_{\text{ext}}$ ). To minimize this path dependency, the models are loaded in small monotonic steps to the prescribed final condition. At each loading step, the inelastic frictional slip along the faults requires iterative solution until the system converges [Cooke and Pollard, 1997]. A user prescribed tolerance is used to assess convergence.

### 3.2. Validation of Numerical Results by Comparison to Analytical Solution

[29] For validation purposes, we first consider the work budget of an unfaulted block (Figure 2). Because there are no faults,  $W_{\text{fric}} = W_{\text{prop}} = W_{\text{seis}} = 0$ , and the entire energy balance equation simplifies to

$$W_{\text{int}} + W_{\text{grav}} = W_{\text{TOT}}; \quad (18a)$$

for energy balanced system,

$$W_{\text{TOT}} = W_{\text{ext}}. \quad (18b)$$

The external work applied along the boundary is partitioned into internal strain energy and uplift against gravity (Table 2). The numerical model total of  $W_{\text{int}}$  and  $W_{\text{grav}}$  is within 0.01% of the external work computed along the boundary, adequately simulating energy-balanced deformation in the unfaulted case. To assess the error of the numerical method we compare the results with analytical solutions for deformation in the deformed block. This comparison illustrates that the  $W_{\text{grav}}$  term incurs the greatest error of <2%. This small error is likely due to sampling and/or discretization effects. We encounter sampling errors because we calculate internal strain energy and gravity by summing over a grid of observation points; the error was reduced by increasing the density of the grid and would be zero for an infinitely dense grid. Discretization effects are due to the treatment of boundary and fault surfaces as a series of elements with uniform displacements and stresses; this error was reduced by reducing the element size (increasing the number of elements). The latter error is likely to increase with consideration of faults in the model, as the amount of discretized area (boundaries plus faults) increases. The error of the faulted models can be assessed indirectly by summing the work terms and comparing to external work; these are reported within subsequent sections. We consider errors within a few percent of the work to be suitably small for this study, thus requiring no further refinement of the model.

## 4. Static One-Fault System

[30] We next consider 6 km long frictional and frictionless faults dipping  $35^\circ$  (Figure 3). For these static models, the faults are not permitted to propagate (i.e.,  $W_{\text{prop}} = 0$ ) and do not experience stick slip resulting in earthquake events, so  $W_{\text{seis}} = 0$ . To minimize the path-dependent effects of the frictional and external work, these models are loaded monotonically in four steps. The model results are set forth in Table 3.

[31] For the frictionless case, the total of  $W_{\text{int}}$  and  $W_{\text{grav}}$  is within 0.1% of the external boundary work; the faulted model is less balanced than in the no fault case. This is likely due to the additional discretization effect along the fault leading to uncertainty in accounting for the internal strain at points near the fault that the BEM cannot reliably calculate. Discretization of the fault into a greater number of smaller elements will reduce this discrepancy; however we consider these errors to be suitably negligible. Addition of the freely slipping fault results in a reduction in the internal strain energy from the no fault case, and an offsetting increase in gravitational work. Adding a fault reduces the internal strain, but at a "cost" of increased work against gravity. The reduction in strain energy is greater than the corresponding increase in the other work terms, so that less total work is required to deform a faulted area than an

**Table 2.** Work Balance for Faultless Case, Comparing Numerical Model and Analytical Results<sup>a</sup>

	$W_{\text{int}}$	$W_{\text{grav}}$	$W_{\text{TOT}}$	$W_{\text{ext}}$
Numerical	976.4	128.8	1104.8	1105.3
Analytical	976.6	130.8	1107.4	1107.4
Error	-0.2	-2.0	-2.2	-2.1

<sup>a</sup> $W_{\text{int}}$  and  $W_{\text{grav}}$  are the only nonzero work components. Work values are in terajoules.



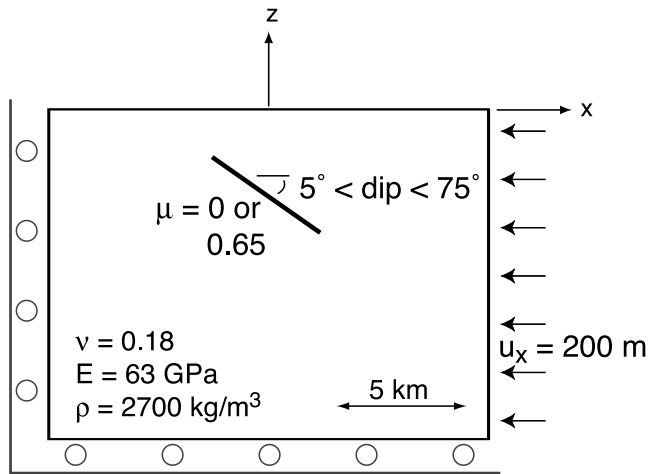


**Figure 3.** Configuration of single-fault model. The friction coefficient along a 35° dipping fault assigned either 0 or 0.65 in order to assess the sensitivity of the work balance to presence of work against friction. In another set of numerical experiments, fault dip varies from 5° to 75° to explore the sensitivity of fault dip on the distribution of work.

544 unfaulted one. Taken to the extreme, we might then expect a  
 545 dense spiderweb-like network of faults to develop in order  
 546 minimize energy; however, the production of fault surface  
 547 area consumes energy. Many small faults have greater  
 548 surface area and require greater  $W_{prop}$  than a few longer  
 549 faults. The energy required for fault propagation is explic-  
 550 itly considered in section 9.

551 [32] We then consider the same fault with a constant  
 552 friction coefficient of 0.65, within the range of friction  
 553 coefficients found in laboratory sliding experiments  
 554 [Byerlee, 1978]. The numerical model continues to produce  
 555 a reasonably close energy-balanced budget (within 0.1%,  
 556 Table 3). The imbalance is similar to that for the frictionless  
 557 fault. As expected, the frictional fault work results lie  
 558 between the end-members of freely slipping and no fault  
 559 models. The frictional fault case requires more energy to  
 560 produce the prescribed strain than the frictionless fault, but  
 561 less energy than the no fault case. The frictional fault  
 562 produces a reduction in  $W_{int}$  from the no-fault case with  
 563 offsetting increases in both  $W_{grav}$  and  $W_{fric}$ .

## 564 5. Frictional Faults at Varying Dips

565 [33] Next, we consider a 6 km frictional fault at varying  
 566 dips. Once again loading is applied over 4 steps and the  
 567 faults are static. For this analysis, we are concerned with the  
 568 relative changes in each work term; accordingly, Figure 4

t3.1 **Table 3.** Work Balance for 35° Dipping Fault Model<sup>a</sup>

t3.2	$W_{int}$	$W_{grav}$	$W_{fric}$	$W_{TOT}$	$W_{ext}$
t3.3 No fault	976.4	128.8	0.0	1105.2	1105.3
t3.4 Frictionless fault	934.2	138.3	0.0	1072.5	1071.9
t3.5 Frictional fault	954.5	132.0	13.0	1099.5	1098.9

t3.6 <sup>a</sup>Frictionless and frictional ( $\mu = 0.65$ ) faults are compared to faultless case. The system is static, with no earthquake events and no fault propagation, so that  $W_{seis}$  and  $W_{prop}$  are zero. Work values are in terajoules.

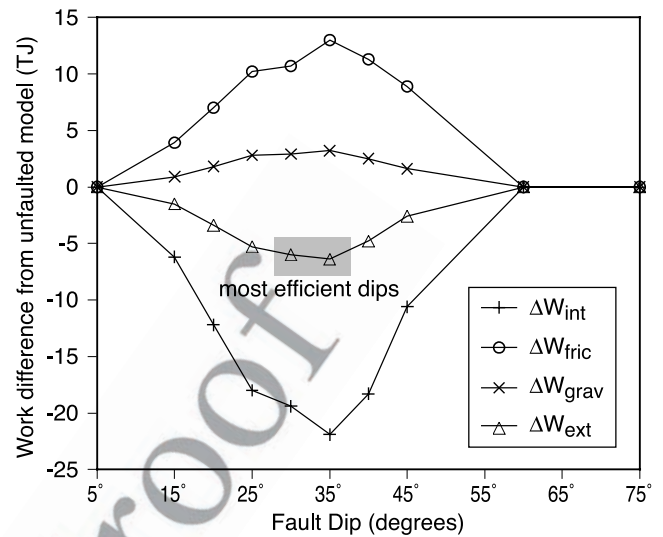


**Figure 4.** Difference for all work components between the faulted and unfaulted models under varying fault dips and 0.65 friction coefficient. Faults with very shallow (dip  $\leq 5^\circ$ ) or steep (dip  $\geq 60^\circ$ ) dips do not slip under the modeled horizontal contraction modeled. The 30°–35° dipping faults have the lowest external ( $W_{ext}$ ) work and are the most efficient fault dips to accommodate horizontal contraction. The 35° fault has lesser internal work ( $W_{int}$ ) and greater work against gravity ( $W_{grav}$ ) than the 30° dipping fault. The most efficient fault dips found here by work minimization fall within the range of faulting observations in triaxial tests (20°–40° [Handin, 1966; Goodman, 1989]).

shows the difference in work components from the 569 unfaulted case. The work terms vary consistently with 570 dip. Addition of any slipping fault reduces the internal 571 strain energy, and produces offsetting increases in frictional 572 and gravitational work. Once again, the reduction in strain 573 energy exceeds the corresponding increase in the other work 574 terms, so that less total work is required to deform faulted 575 regions than unfaulted ones. However, unfavorably oriented 576 faults, i.e., faults that do not slip, do not reduce the total 577 work. 578

[34] The premise of work minimization leads us to expect 579 that the faults most likely to develop within an evolving 580 system would be those requiring the least work to accom- 581 modate the same tectonic strain. Our model shows that 582 faults dipping 30°–35° require the least external work. The 583 35° dipping fault has lesser internal work than the 30° 584 dipping fault, but this work benefit is tempered by the 585 greater work expended against gravity for the 35° dipping 586 fault. These fault dips are within the range of failure surface 587 orientations observed in triaxial tests [e.g., Handin, 1966; 588 Goodman, 1989]. Furthermore, the most efficient fault dips 589 may depend on friction coefficient. For example, freely 590 slipping faults are expected to provide the greatest energy 591 savings at 45° dip, the plane of maximum shear stress under 592 horizontal contraction. 593

## 6. Consideration of Seismic Energy Release 594

[35] The work budgets in section 5 describe faults that do 595 not experience earthquake events; these creeping faults 596

radiate no seismic energy because the faults are constantly responding to the resolved stress state. Although the BEM model does not explicitly include earthquake events, we can calculate the seismic energy that would be released if, for each tectonic loading step, the slip on all faults within the model occurred in a single earthquake event. To do this, we compare the total work required to strain the faultless model, equivalent to a locked fault, to the external work required for the faulted model. The change in energy,  $\Delta W_{\text{ext}}$ , reflects the seismic work released due to the fault slip.

[36] Alternatively, the seismic energy released can be calculated directly using equation (14) by integrating over the tectonic loading the fault slip and associated change in shear stress. For each loading step, we calculate the change in slip from the previous step and the drop in shear stress before and after slip. As with the  $\Delta W_{\text{ext}}$  method, all faults are assumed to slip in one earthquake during each loading step and the shear stress drop is assumed to occur linearly throughout the modeled slip (Figure 5a).

[37] In order to assess the accuracy of the two methods, we compare the change in external work to the direct calculation of seismic work for a  $35^\circ$  dipping frictionless fault (Table 4). For this case,  $\Delta W_{\text{ext}}$  is within several terajoules of the calculated  $W_{\text{seis}}$ . This difference is similar to the error of the numerical calculations of  $W_{\text{ext}}$  (Table 2) so that either method can be used to calculate seismic energy released. For these creeping faults, we prefer calculating  $\Delta W_{\text{ext}}$  because of the ease of computation.

[38] The calculations of seismic energy from the fault models represent a maximum potential release of seismic energy because dynamic stress drops during slip are not considered. The calculations of seismic energy assume that the shear stress drop associated with the earthquake occurs linearly throughout the slip of the earthquake event (Figure 5a). However, laboratory studies have shown that dynamic stress drops are focused at the onset of slip [e.g.,

**Table 4.** Seismic Energy Released for a Frictionless  $35^\circ$  Dipping Fault<sup>a</sup>

	$W_{\text{ext}}$ , TJ	$\Delta W_{\text{ext}}$ , TJ	Calculated Seismic Energy, TJ
No fault	1105.3		
Frictionless	1071.9	33.4	36.4

<sup>a</sup>Calculated seismic energy (equation (14)) is compared to change in external energy between preearthquake (locked or no fault) and postearthquake (frictionless) cases.

Dieterich, 1979] (Figure 5b). If the shear stress drop occurs over a smaller slip, lesser seismic energy is released even though the total work of the system is unchanged. The ratio of seismic energy released in earthquakes and laboratory slip events to the energy available has been expressed as seismic efficiency,  $\eta$  [e.g., *McGarr*, 1999]. Within this study, we have neglected dynamic stress drops so that  $\eta = 1$  and the seismic energy released equals the change in total work ( $W_{\text{seis}} = \Delta W_{\text{ext}}$ ). However, earthquakes and laboratory slip events have been shown to have seismic efficiencies smaller than 0.06 [*McGarr*, 1994, 1999]. We should note that here we calculate the change in total work of the system as the available energy, whereas *McGarr* [1999] uses the change in internal energy ( $W_{\text{int}}$ ). These formulations are identical if work against gravity ( $W_{\text{grav}}$ ) and frictional heating ( $W_{\text{fric}}$ ) are assumed to be negligible.

## 7. Consideration of Fault Propagation

[39] In order to explore the final component of the work budget,  $W_{\text{prop}}$ , and its implications for studying fault system evolution, we consider the propagation of a fault in our simple one fault system. Starting with our single 6 km long fault dipping  $35^\circ$  we propagate the fault in two directions in alternative models. The first extends the original fault 1 km toward the surface, maintaining a dip of  $35^\circ$ . The second propagates as a 1 km long back thrust, initiating at the midpoint of the original fault, and dipping  $35^\circ$  in the opposite direction (Figure 6).

[40] As expected, the extension of the original fault reduces the total work required to produce the prescribed displacement on the boundary (Figure 6b). As with the previous models, addition of the slipping fault surface reduces  $W_{\text{int}}$  and increases  $W_{\text{grav}}$  and  $W_{\text{fric}}$ , with a lower total work,  $W_{\text{ext}}$ .

[41] In contrast, addition of a back thrust does not reduce the total work. A small degree of reverse slip on the back thrust reduces  $W_{\text{int}}$  but also increases work against friction ( $W_{\text{fric}}$ ) and work against gravity ( $W_{\text{grav}}$ ) relative to the original fault system. Using our criteria that we would only expect fault growth that decreases the total work of the system, we would expect extension of the original fault rather than development of a back thrust under our model conditions. Other studies suggest that back thrusts may only be favored in conditions with interlayer slip [*Nino et al.*, 1998] or under specific conditions of topography and erosion [*Masek and Duncan*, 1998].

[42] While extension of the original fault reduces total work in the static energy balance, the cost of this fault propagation is not accounted for in that balance: Energy is required to break the rock and create new fault surface ( $W_{\text{prop}}$ ). The overall efficiency of the system is only

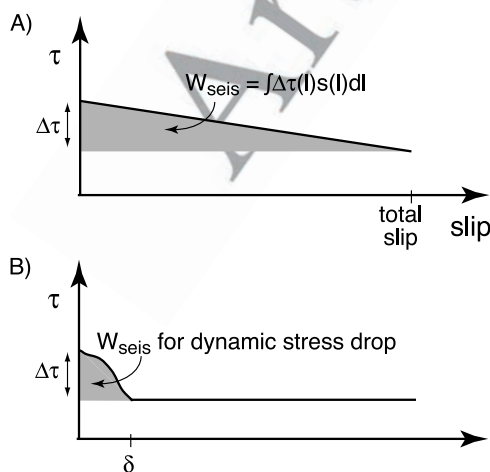


**Figure 5.** Comparison of seismic energy release from (a) one tectonic loading step within the loading path integral of equation (14) and (b) one slip event (earthquake) with dynamic shear stress drop. The seismic energy released is the grey area under the  $\tau$  slip curve. The  $\delta$  represents the critical slip distance over which the friction evolves to steady state.



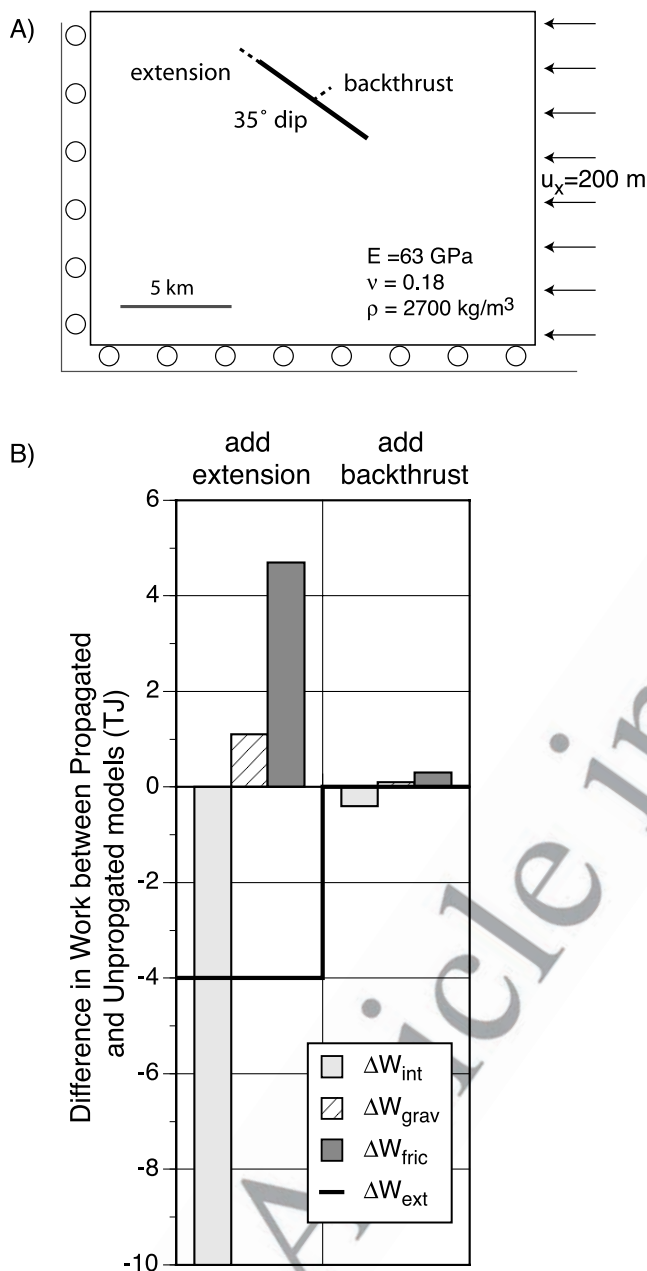


**Figure 6.** (a) Alternative propagation paths of a 35° dipping two-dimensional fault include (1) extension within the plane of the fault or (2) development of a back thrust. (b) Propagation by extension of the fault provides a greater energy savings than propagation by back thrusting. The systemic energy savings of 4 TJ achieved by extending the fault exceeds laboratory estimates of the energy required to create the new fault surface,  $W_{\text{prop}}$ .

690 increased if the energy saved by extension of the fault  
691 exceeds the energy required to create the fault.

692 [43] Following *Mitra and Boyer* [1986], we use the  
693 relationship of (15) to estimate  $W_{\text{prop}}$ . Experimental studies  
694 have shown that the critical surface energy values,  $\gamma$ , for  
695 various rock types, depend on normal compression and  
696 range from  $10^1$  to  $0^4 \text{ J m}^{-2}$  [*Wong*, 1982, 1986; *Cox and*  
697 *Scholz*, 1988]. Because mode III fault propagation generally

shows  $\gamma$  at the lower end of this range  $10^1 - 10^2 \text{ J m}^{-2}$  [*Cox* 698  
*and Scholz*, 1988], a higher surface energy should be 699  
considered for the mode II propagation simulated in this 700  
study. The thickness of the granulated fault zones has been 701  
estimated as 1/10 to 1/100 the fault displacement 702  
[*Robertson*, 1983; *Scholz*, 1987]. *Mitra and Boyer* [1986] 703  
use  $500 \text{ m}^{-1}$  for the density of secondary faults in the 704  
cataclastic zone. 705

[44] Substituting these values into (15) for added fault 706  
length of 1 km with maximum displacement of 23 m, gives 707  
a  $W_{\text{prop}}$  of  $\sim 1 - 11 \text{ GJ}$ . Even though this analysis includes 708  
consideration of a cataclastic fault zone, the energy required 709  
to propagate the fault is several orders of magnitude smaller 710  
than the change in efficiency (Figure 6), which is on the 711  
order of Terajoules. Thus the fault propagation energy is 712  
insignificant compared to the other forms of work energy, 713  
consistent with the findings of *Mitra and Boyer* [1986] and 714  
the analytical calculations of *Scholz* [2002]. This indicates 715  
that for the tectonic contraction modeled here, growth of a 716  
fault extension of this length would easily be favored under 717  
efficiency criteria. 718

## 8. Application of Two-Dimensional Work Budget 719 to the Los Angeles Basin 720

[45] The final application of the work balance method 721  
considers a transect across the Los Angeles Basin. The Los 722  
Angeles Basin is undergoing active crustal deformation 723  
expressed as slip along a three-dimensional system of 724  
interacting faults [e.g., *Yerkes*, 1965; *Davis et al.*, 1989; 725  
*Wright*, 1991; *Shaw and Suppe*, 1996; *Shen et al.*, 1996; 726  
*Walls et al.*, 1998]. Sets of active NW trending faults 727  
(including the Whittier, Newport-Inglewood and Palos 728  
Verdes faults) and E-W trending faults (including the 729  
Malibu-Santa Monica-Raymond Hill fault system) are be- 730  
lieved to interact via a subsurface system of horizontal 731  
detachments and thrust ramps at  $\sim 10 - 15 \text{ km}$  depth [*Davis* 732  
*et al.*, 1989; *Shaw and Suppe*, 1996]. 733

[46] We consider a two-dimensional model of faults in the 734  
Los Angeles basin along a cross section from the Palos 735  
Verdes Hills to the Whittier Hills (Figure 7a). The subsur- 736  
face fault geometry (Figure 7b) is based on kinematic 737  
inferences from overlying fault shape [*Shaw and Suppe*, 738  
1996]. A 0.5% contraction, applied by translating the right 739  
side of the model, represents  $\sim 50,000$  years of contraction 740  
at current strain rates [e.g., *Argus et al.*, 1999; *Bawden et* 741  
*al.*, 2001]. We consider two models, one with frictionless 742  
faults and a second with faults having a uniform friction 743  
coefficient of 0.4, which simulates mature fault surfaces 744  
weakened by fluids and falls within the range of values 745  
suggested by previous researchers [*Deng and Sykes*, 1997; 746  
*King et al.*, 1994; *Scholz*, 2000; *Cooke and Kameda*, 2002]. 747  
To minimize the path-dependent effects of the frictional and 748  
external work, these models are loaded monotonically in 749  
eight steps. At each step, the model solution is iterated to 750  
convergence so that the faults are in equilibrium with their 751  
surrounding stress state. 752

[47] Even with a far more complex network of faults than 753  
presented thus far, the work budget is reasonably close to 754  
being energy balanced (i.e.,  $W_{\text{TOT}} \sim W_{\text{ext}}$ ; Figure 8a). The 755  
imbalance is 7.3% for the frictionless case and 0.5% for the 756  
frictional case. 757

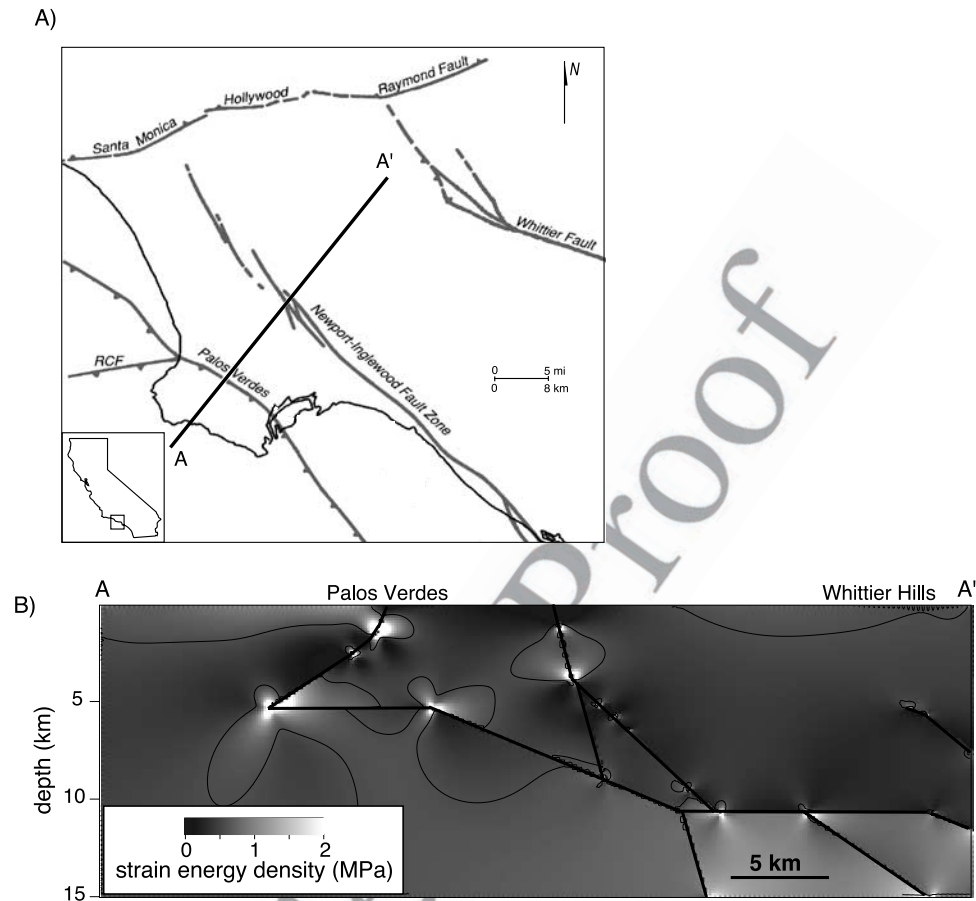


**Figure 7.** (a) Fault map of the Los Angeles Basin, California. The bold line marks the approximate trace of the cross section studied (modified from *Wright* [1991] and *Cooke and Kameda* [2002]). (b) Fault model showing distribution of internal strain around the freely slipping faults. The average strain energy density for the model (0.58 MPa) is contoured. Bright regions have greater than average internal strain whereas dark areas are in the strain shadows of slipping faults.

758 [48] As expected, the reduction in total work from an  
 759 unfaulted case is far greater for a frictionless fault network  
 760 than for the frictional faults, due to far greater slip occurring  
 761 on faults when they slip freely (Figure 8b). Although the  
 762 frictionless faults exhibit greater uplift against gravity, as a  
 763 consequence of greater fault slip, the drop in  $W_{\text{int}}$  more than  
 764 compensates for the increase in work against gravity,  $W_{\text{grav}}$ .  
 765 In addition to the greater reduction in  $W_{\text{int}}$ , faults that slip  
 766 completely freely require no work against friction to ac-  
 767 commodate sliding deformation.

768 [49] The energy balance continues to be dominated by  
 769 the internal strain energy. In the frictional faults case, the  
 770 work expended overcoming frictional resistance is  $\sim 2\%$  of  
 771 the work expended in internal strain energy. This suggests  
 772 that far less energy may be transferred to heat flow than to  
 773 uplift and deformation of host rock. However, the propor-  
 774 tions of internal work to frictional work and seismic work  
 775 should be considered in the context of the simplistic two-  
 776 dimensional deformation of the models. Contraction across  
 777 the Los Angeles basin is accommodated by strike-slip as  
 778 well as reverse slip so that three-dimensional models  
 779 incorporating strike slip may produce greater  $W_{\text{fric}}$  and  
 780 lesser  $W_{\text{int}}$  than two-dimensional models. The partitioning

of work components is discussed further in section 9 of 781  
 this paper.

[50] We can calculate the cumulative seismic energy that 783  
 would be released if all of the faults slipped within in a 784  
 single earthquake event per loading step. The following 785  
 relationship can be used to calculate the equivalent earth- 786  
 quake moment,  $M_S$ , from the seismic energy released,  $W_{\text{seis}}$ , 787  
 [e.g., *Scholz*, 2002] 788

$$M_S = 2/3 \log(W_{\text{seis}}) - 3.2. \quad (19)$$

If the faults slipped without frictional resistance in 790  
 one earthquake event over the modeled time period 791  
 (50,000 years), 23 TJ of seismic energy would be released 792  
 equivalent to a  $M$  5.7 earthquake. If the faults slipped 793  
 frictionally in one earthquake, 6 TJ of seismic energy would 794  
 be released, equivalent to a  $M$  5.3 earthquake. We can 795  
 incorporate the reduction in seismic energy expected from 796  
 dynamic shear stress drop by implementing a seismic 797  
 efficiency of 0.06 [e.g., *McGarr*, 1999]. The expected 798  
 earthquake magnitude drops to  $M$  4.9 for the frictionless and 799  
 to  $M$  4.5 for the frictional cases. 800

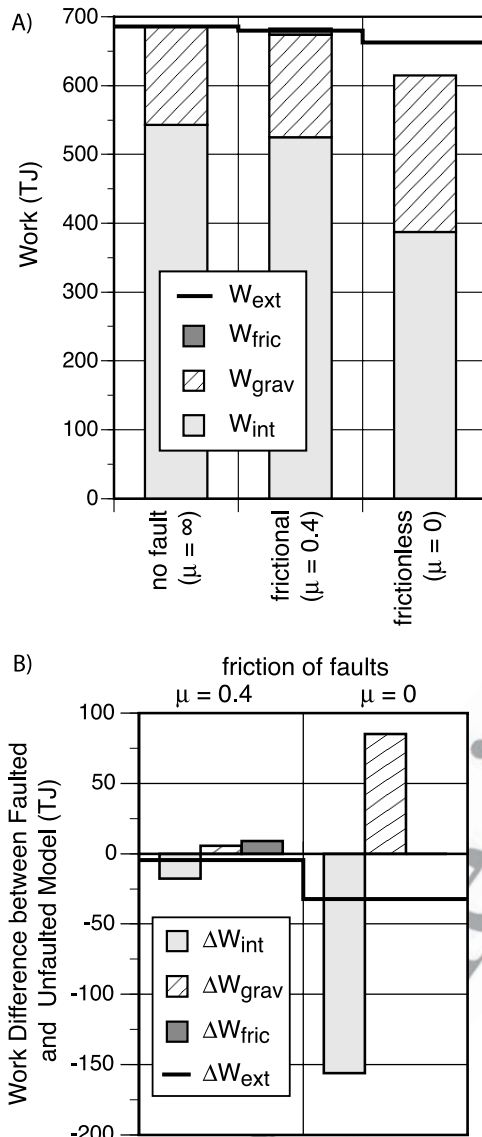


**Figure 8.** (a) Distribution of work within a two-dimensional system of faults simulating the Los Angeles Basin. Under frictional conditions ( $\mu = 0.4$ ), many faults have limited or negligible slip. Consequently, frictional heating is small and the other work terms resemble results of the unfaulted model. (b) The difference in all work terms between the faulted and unfaulted models. The frictionless fault model is more efficient than the frictional faults despite the added work against gravity, which would be expressed as uplift. The change in external work,  $\Delta W_{ext}$ , serves as a proxy for seismic energy released if all the faults within the model slipped in one event within 50,000 years. The frictionless faults release greater seismic energy than the frictional faults.

801 [51] These hypothetical calculations do not reflect accurate earthquake hazards for the region. Because we have modeled only a two-dimensional cross section, we are neither considering the complete three-dimensional slip vector nor considering the complete fault surface area at risk to slipping in earthquake events; consequently, two-dimensional analyses understate the maximum potential for

808 seismic energy release. On the other hand, all of the faults are not expected to release 50,000 years of stored energy within a single earthquake event. These calculations overstate the earthquake magnitude expected from events that occur on subsets of the regional faults over recurrence time periods less than 50,000 years. 813

## 9. Discussion 814

[52] A work balance approach to examining fault systems holds great potential for allowing analysis of entire systems of interacting faults and understanding fault system evolution. The numerical models allow us to evaluate the work done on the boundary of a complex system without requiring a detailed analysis of every component of work within the system. This can provide a benefit where the major issue of concern is the overall work required to deform the system, such as in assessing overall fault system efficiency, or providing an overall estimate of seismic energy potential. 824

### 9.1. Partitioning of Work 825

[53] The energy budgets are dominated by internal strain energy, even in the Los Angeles Basin model, a region with substantial faulting. Gravitational work also presents a substantial component of the total work, whereas relatively little energy is expended overcoming frictional resistance. 830

[54] That is not to say that the influence of frictional work is unimportant, especially when considering the evolution of a system along alternative paths of faulting. While  $W_{int}$  is by far the largest work component, the changes in  $W_{int}$  among models with differing fault geometries are comparable in magnitude to the changes in  $W_{grav}$  and the total frictional work  $W_{fric}$  (Figures 4, 6, and 8b). If this were not the case, the work budget would not balance. In our models, then, the path of deformation is being influenced by energy factors that represent a relatively small proportion of the total energy input into the system. 841

[55] Within natural systems, other processes may contribute to the energy of the system that are not considered here. Chemical reactions such as those that facilitate pressure solution and other inelastic deformation may act to alter the internal work and the external work on the system. Inelastic deformation likely in regions of high internal strain (e.g., bright regions on Figure 7b) may reduce the stress terms in the equations for both  $W_{int}$  and  $W_{ext}$  and may increase the strain terms within  $W_{int}$ . If the stress-strain relations for the inelastic processes are known, they can be considered explicitly within  $W_{int}$  (equation (6)) and linear elasticity need not be assumed. 853

[56] It is possible that the partitioning of work will change as a fault system matures. A fault system in its earliest stages may have a work budget that resembles that of an unfaulted system. In that case, it would be unsurprising that the single-fault models have work budgets dominated by  $W_{int}$ . As a matter of efficiency, we expect that a more mature fault system will have a lower total work; we might also expect that the partitioning of work would be different, with less work expressed as  $W_{int}$  and more expressed as gravitational work. 863

[57] We see some evidence for reduction of internal work in our models of extension of the  $35^\circ$  dipping fault, and of the complex Los Angeles fault network. The extension of 866



867 the fault reduces total work by reducing  $W_{\text{int}}$  and increasing  
 868  $W_{\text{grav}}$  and  $W_{\text{fric}}$ ; while both the total work and  $W_{\text{int}}$  decrease,  
 869  $W_{\text{int}}$  is a smaller proportion of the total work for the  
 870 extended fault than for the initial fault (86% < 87%).  
 871 Similarly, in the Los Angeles model the percentage of the  
 872 work budget consumed in internal strain energy decreases  
 873 from the unfaulted model (79%) to the frictional fault model  
 874 (77%) to the frictionless model (58%). The partitioning of  
 875 work among forms of deformation therefore may be an  
 876 indicator of the maturity of fault systems.

## 877 9.2. Assessing Between Alternative Fault System 878 Configurations

879 [58] A major focus of previous work analyses has been in  
 880 determining efficient or minimum work paths of deformation  
 881 [Masek and Duncan, 1998; Jamison, 1993; Dahlen and  
 882 Barr, 1989; Molnar and Lyon-Caens, 1988; Mitra and  
 883 Boyer, 1986; Sleep et al., 1979]; elements of the work  
 884 analysis here have been applied for that purpose [Cooke and  
 885 Kameda, 2002; Griffith and Cooke, 2004]. The more  
 886 complete analysis presented here presents evidence in  
 887 support of these applications. The energy minimization  
 888 analysis of faults with varying dip found that 30°–35°  
 889 dipping faults were the most energy efficient, consistent  
 890 with experimental observations. The energy minimization  
 891 analysis for alternative fault propagation paths preferred  
 892 fault extension rather than back thrust development, which  
 893 has been shown to require heterogeneous conditions.

894 [59] Although these simple models assume homogeneous  
 895 rheology, in many regions of the Earth we expect increasing  
 896 stiffness with depth and/or lateral variations in material  
 897 properties. Such heterogeneities are expected to locally alter  
 898 the stress field so that predictions of efficient fault config-  
 899 uration for a homogenous region may not be applicable to  
 900 heterogeneous region. However, even within regions with  
 901 heterogeneous material properties, the first-order heteroge-  
 902 neities controlling deformation may be the fault surfaces/  
 903 zones, which serve to localize deformation.

904 [60] These results presented in this study demonstrate that  
 905 the minimum work approach can successfully assess be-  
 906 tween both alternative fault geometry and/or alternative  
 907 fault propagation paths. Consequently, these work minimi-  
 908 zation tools might also be used to predict the propagation  
 909 and evolution of fault systems.

## 910 9.3. Implications for Earthquake Assessments

911 [61] Our calculations of potential seismic energy release  
 912 based on creeping faults can provide an upper bound to  
 913 earthquake seismic moment assessments; the calculations  
 914 presume 1) that all of the seismic energy in the modeled  
 915 increment of deformation is released in a single earthquake  
 916 event and 2) that the shear stress drop occurs throughout the  
 917 slip event. Although the modeled faults within this study all  
 918 slip together during each tectonic loading step, earthquakes  
 919 are generally temporally distributed on individual faults or  
 920 fault segments. Tectonic loading steps smaller than typical  
 921 earthquake recurrence intervals (<1000 years) could limit  
 922 slip events at each step to those fault surfaces that are  
 923 critically stressed. Alternatively, because earthquakes seem  
 924 to have a relatively consistent stress drop of  $\sim 3$  MPa  
 925 [Abercrombie, 1995], we could allow faults to slip when-  
 ever the potential shear stress drop exceeds 3 MPa. The

second presumption can be accommodated to some degree 927  
 by using observations of seismic efficiency from earth- 928  
 quakes and laboratory slip events to reduce  $W_{\text{seis}}$ . Seismic 929  
 efficiency provides a basis for calculating the apparent 930  
 seismic energy released from the total energy available 931  
 [McGarr, 1999]. 932  
 933

## 10. Conclusions 934

[62] The work budget gives a sense of the partitioning of 935  
 tectonic work among various forms of deformation: fric- 936  
 tional heating, uplift, tectonic deformation, fault growth and 937  
 seismic energy release. The BEM models are shown to 938  
 produce a balanced work budget for both simple and 939  
 complex fault system models. Deformation through fault 940  
 slip permits a region to accommodate tectonic strain with 941  
 less work done in the form of internal strain of the rock, but 942  
 at a cost in terms of work resisting friction and increased 943  
 work against gravity. Generally, the addition of slipping 944  
 faults reduces the work required to accommodate tectonic 945  
 strain. We see large differences in work energy saved by the 946  
 addition of faults depending on fault rheology. Systems 947  
 requiring less work are considered more efficient than those 948  
 requiring greater work, and the system requiring a minimum 949  
 of work would be favored under efficiency considerations. 950  
 Calculations of minimum work deformation are shown 951  
 to match expected deformation paths, indicating the useful- 952  
 ness of this approach for evaluating efficiency in more 953  
 complex systems. A work balance approach to examining 954  
 fault systems holds great potential for allowing analysis of 955  
 entire systems of interacting faults and understanding fault 956  
 system evolution. 957

[63] **Acknowledgments.** This manuscript greatly benefited from our 958  
 discussions with Gautam Mitra, Heather Savage, and Jon Lewis as well as 959  
 from comments of two anonymous reviewers. Graduate fellowships from 960  
 both the University of Massachusetts Graduate School and the National 961  
 Science Foundation provided support for Susan Murphy. 962

## References 963

- Abercrombie, R. E. (1995), Earthquake source scaling relationships from – 964  
 1 to 5 M (sub L) using seismograms recorded at 2.5-km depth, *J. Geo-* 965  
*phys. Res.*, *100*, 24,015–24,036. 966  
 Argus, D. F., et al. (1999), Shortening and thickening of metropolitan Los 967  
 Angeles measured and inferred by using geodesy, *Geology*, *27*, 703–706. 968  
 Bawden, G. W., W. Thatcher, R. S. Stein, K. W. Hudnut, and G. Peltzer 969  
 (2001), Tectonic contraction across Los Angeles after removal of ground- 970  
 water pumping effects, *Nature*, *412*, 812–815. 971  
 Buczkowski, D. L., and M. L. Cooke (2004), Formation of double-ring 972  
 circular grabens due to volumetric compaction over buried impact craters: 973  
 Implications for thickness and nature of cover material in Utopia Planitia, 974  
 Mars, *J. Geophys. Res.*, *109*, E02006, doi:10.1029/2003JE002144. 975  
 Byerlee, J. D. (1978), Friction of rocks, *Pure Appl. Geophys.*, *119*, 615– 976  
 626. 977  
 Childs, C., et al. (2003), The growth and propagation of synsedimentary 978  
 faults, *J. Struct. Geol.*, *25*, 633–648. 979  
 Cohen, S. (1984), Crustal deformation, the earthquake cycle, and models of 980  
 viscoelastic flow in the asthenosphere, *Geophys. J. R. Astron. Soc.*, *78*, 981  
 735–750. 982  
 Cooke, M. L., and A. Kameda (2002), Mechanical fault interaction within 983  
 the Los Angeles Basin: A two-dimensional analysis using mechanical 984  
 efficiency, *J. Geophys. Res.*, *107*(B7), 2146, doi:10.1029/2001JB000542. 985  
 Cooke, M., and D. Pollard (1997), Bedding-plane slip in initial stages of 986  
 fault-related folding, *J. Struct. Geol.*, *19*, 567–581. 987  
 Cooke, M., and C. Underwood (2001), Fracture termination and step-over 988  
 at bedding surfaces due to frictional slip and interface debonding, 989  
*J. Struct. Geol.*, *23*, 223–238. 990  
 Cooke, M., P. Mollema, D. Pollard, and A. Aydin (2000), Interlayer slip and 991  
 joint localization in East Kaibab Monocline, Utah: Field evidence and 992  
 results from numerical modeling, in *Forced Folds and Associated Frac-* 993

- 994 tures, edited by J. W. Cosgrove and M. S. Ameen, *Geol. Soc. Spec. Publ.*, 1058  
995 169, 23–49. 1059
- 996 Cox, S. J. D., and C. H. Scholz (1988), Rupture initiation in shear fracture 1060  
997 of rocks: An experimental study, *J. Geophys. Res.*, 93, 3307–3320. 1061
- 998 Crouch, S. L., and A. M. Starfield (1990), *Boundary Element Methods in* 1062  
999 *Solid Mechanics*, Unwin Hyman, Boston, Mass. 1063
- 1000 Dahlen, F. A., and T. D. Barr (1989), Brittle frictional mountain building: 1064  
1001 1. Deformation and mechanical energy budget, *J. Geophys. Res.*, 94, 1065  
1002 3906–3922. 1066
- 1003 Davis, T. L., J. Namson, and R. F. Yerkes (1989), A cross section of the Los 1067  
1004 Angeles area; seismically active fold and thrust belt, the 1987 Whittier 1068  
1005 Narrows earthquake, and earthquake hazard, *J. Geophys. Res.*, 94, 9644– 1069  
1006 9664. 1070
- 1007 Dawers, N. H., and J. R. Underhill (2000), The role of fault interaction and 1071  
1008 linkage in controlling synrift stratigraphic sequences: Late Jurassic, Staff- 1072  
1009 jord East area, northern North Sea, *AAPG Bull.*, 84(1), 45–64. 1073
- 1010 Deng, J., and L. R. Sykes (1997), Evolution of the stress field in southern 1074  
1011 California and triggering of moderate-sized earthquakes: A 200-year per- 1075  
1012 spective, *J. Geophys. Res.*, 102, 9859–9886. 1076
- 1013 Dieterich, J. H. (1979), Modeling of rock friction: 1. Experimental results 1077  
1014 and constitutive equations, *J. Geophys. Res.*, 84, 268–2161. 1078
- 1015 Du, Y., and A. Aydin (1993), The maximum distortional strain energy 1079  
1016 density criterion for shear fracture propagation with applications to the 1080  
1017 growth paths of en echelon faults, *Geophys. Res. Lett.*, 20, 1091–1094. 1081
- 1018 Engelder, T. (1993), *Stress Regimes in the Lithosphere*, Princeton Univ. 1082  
1019 Press, Princeton, N. J. 1083
- 1020 Goodman, R. (1989), *Introduction to Rock Mechanics*, 2nd ed., 562 pp., 1084  
1021 John Wiley, Hoboken, N. J. 1085
- 1022 Griffith, W. A., and M. Cooke (2004), Mechanical validation of the three- 1086  
1023 dimensional intersection geometry between the Puente Hills blind thrust 1087  
1024 system and the Whittier fault, Los Angeles, CA, *Bull. Seismol. Soc. Am.*, 1088  
1025 94, 493–505. 1089
- 1026 Gupta, S., P. A. Cowie, N. H. Dawers, and J. R. Underhill (1998), A 1090  
1027 mechanism to explain rift-basin subsidence and stratigraphic patterns 1091  
1028 through fault array evolution, *Geology*, 26, 595–598. 1092
- 1029 Handin, J. (1966), Strength and ductility, in *Handbook of Physical Con-* 1093  
1030 *stants*, edited by J. S. P. Clark, *Mem. Geol. Soc. Am.*, 97, 223–290. 1094
- 1031 Harris, R. A. (1998), Stress triggers, stress shadows, and implications for 1095  
1032 seismic hazard, Introduction to the special issue, *J. Geophys. Res.*, 103, 1096  
1033 24,347–24,358. 1097
- 1034 Jaeger, J. C., and N. G. W. Cooke (1976), *Fundamentals of Rock* 1098  
1035 *Mechanics*, John Wiley, Hoboken, N. J. 1099
- 1036 Jamison, W. R. (1993), Mechanical stability of the triangle zone; the back- 1100  
1037 thrust wedge, *J. Geophys. Res.*, 98, 20,105–20,030. 1101
- 1038 Kattenhorn, S. A., and D. D. Pollard (2001), Integrating 3-D seismic data, 1102  
1039 field analogs, and mechanical models in the analysis of segmented nor- 1103  
1040 mal faults in the Wytch Farm oil field, southern England, United King- 1104  
1041 dom, *AAPG Bull.*, 85(7), 1183–1210. 1105
- 1042 King, G. C. P., R. S. Stein, and J. Lin (1994), Static stress changes and the 1106  
1043 triggering of earthquakes, *Bull. Seismol. Soc. Am.*, 84(3), 935–953. 1107
- 1044 Lawn, B. R., and T. R. Wilshaw (1975), *Fracture of Brittle Solids*, Cam- 1108  
1045 bridge Univ. Press, New York. 1109
- 1046 Maerten, L., E. J. M. Willmose, D. D. Pollard, and K. Rawnsley (1999), 1110  
1047 Slip distributions on intersecting normal faults, *J. Struct. Geol.*, 21(3), 1111  
1048 259–271. 1112
- 1049 Mansfield, C., and J. Cartwright (2001), Fault growth by linkage: Observa- 1113  
1050 tion and implications from analogue models, *J. Struct. Geol.*, 23, 745– 1114  
1051 763. 1115
- 1052 Marone, C. (1998), Laboratory-derived friction laws and their application to 1116  
1053 seismic faulting, *Annu. Rev. Earth Planet Sci.*, 26, 643–696. 1117
- 1054 Masek, J. G., and C. C. Duncan (1998), Minimum-work mountain building, 1118  
1055 *J. Geophys. Res.*, 103, 907–917. 1119
- 1056 McGarr, A. (1994), Some comparisons between mining-induced and 1120  
1057 laboratory earthquakes, *Pure Appl. Geophys.*, 142, 467–489. 1121
- McGarr, A. (1999), On relating apparent stress to the stress causing earth- 1058  
quake fault slip, *J. Geophys. Res.*, 104, 3003–3011. 1059
- Mitra, G., and S. E. Boyer (1986), Energy balance and deformation 1060  
mechanisms of duplexes, *J. Struct. Geol.*, 8, 291–304. 1061
- Molnar, P., and H. Lyon-Caens (1988), Some simple physical aspects 1062  
of the support, structure, and evolution of mountain belts, in *Processes* 1063  
in *Continental Lithospheric Deformation*, edited by S. P. Clark Jr., 1064  
C. B. Burchfiel, and J. Suppe, *Spec. Pap. Geol. Soc. Am.*, 218, 197–207. 1065
- Nino, F., H. Philip, and J. Chery (1998), The role of bed-parallel slip in the 1066  
formation of blind thrust faults, *J. Struct. Geol.*, 20, 503–516. 1067
- Robertson, E. C. (1983), Relationship of fault-displacement to gouge and 1068  
breccia thickness, *Min. Eng.*, 35, 1426–1432. 1069
- Roering, J., M. Cooke, and D. D. Pollard (1997), Why blind thrust faults 1070  
don't propagate to the Earth's surface: Numerical modeling of coseismic 1071  
deformation associated with thrust-related anticlines, *J. Geophys. Res.*, 1072  
102, 11,901–11,912. 1073
- Rundle, J. (1982), Viscoelastic-gravitational deformation by a rectangular 1074  
thrust fault in a layered Earth, *J. Geophys. Res.*, 87, 7787–7796. 1075
- Savage, H. M., and M. L. Cooke (2004), An investigation into the role of 1076  
fault interaction on fold pattern, *J. Struct. Geol.*, 26, 905–917. 1077
- Scholz, C. H. (1987), Wear and gouge formation in brittle faulting, *Geol-* 1078  
ogy, 15, 493–495. 1079
- Scholz, C. H. (2000), Evidence for a strong San Andreas fault, *Geology*, 1080  
28(2), 163–166. 1081
- Scholz, C. H. (2002), *The Mechanics of Earthquakes and Faulting*, Cam- 1082  
bridge Univ. Press, New York. 1083
- Shaw, J. H., and J. Suppe (1996), Earthquake hazard of active blind-thrust 1084  
faults under the central Los Angeles basin, California, *J. Geophys. Res.*, 1085  
101, 8623–8642. 1086
- Shen, Z. K., D. D. Jackson, and B. X. Ge (1996), Crustal deformation 1087  
across and beyond the Los Angeles Basin from geodetic measurements, 1088  
*J. Geophys. Res.*, 101, 27,957–27,980. 1089
- Sleep, N. H., S. Stein, R. J. Geller, and R. G. Gordon (1979), The use of 1090  
the minimum-dissipation principle in tectonophysics: Discussion, *Earth* 1091  
*Planet. Sci. Lett.*, 45(1), 218–220. 1092
- Stein, R. S. (1999), The role of stress transfer in earthquake occurrence, 1093  
*Nature*, 402, 605–609. 1094
- Timoshenko, S. P., and J. N. Goodier (1934), *Theory of Elasticity*, McGraw- 1095  
Hill, New York. 1096
- Walls, C., T. Rockwell, K. Mueller, Y. Bock, S. Williams, J. Pfanner, 1097  
J. Dolan, and P. Fang (1998), Escape tectonics in the Los Angeles me- 1098  
tropolitan region and implications for seismic risk, *Nature*, 364, 356–360. 1099
- Willense, E. J. M., and D. D. Pollard (2000), Normal fault growth: evolu- 1100  
tion of tipline shapes and slip distribution, in *Aspects of Tectonic Fault-* 1101  
*ing*, edited by F. K. Lehner and J. L. Urai, pp. 193–226, 1102  
Springer-Verlag, New York. 1103
- Wong, T. F. (1982), Shear fracture energy of Westerly granite from post- 1104  
failure behavior, *J. Geophys. Res.*, 87, 990–1000. 1105
- Wong, T. F. (1986), On the normal stress dependence of the shear fracture 1106  
energy, in *Earthquake Source Mechanics*, *Geophys. Monogr. Ser.*, vol. 1107  
37, edited by S. Das, J. Boatwright, and C. Scholz, pp. 1–12, AGU, 1108  
Washington, D. C. 1109
- Wright, T. L. (1991), Structural geology and tectonic evolution of the Los 1110  
Angeles Basin, California, in *Active Margin Basins*, edited by K. T. 1111  
Biddle, *AAPG Mem.*, 52, 35–134. 1112
- Yerkes, R. F. (1965), Geology of the Los Angeles Basin, California: An 1113  
introduction, *U.S. Geol. Surv. Prof. Pap.*, 0420–A, A1–A57. 1114
- Young, H. D., and R. A. Freedman (1996), *University Physics*, 9th ed., 1115  
Addison-Wesley, Reading, Mass. 1116
- M. L. Cooke and S. Murphy, Geosciences Department, University of 1118  
Massachusetts, Amherst, MA 01003, USA. (cooke@geo.umass.edu) 1119